Colloid Polym Sci (2011) 289:613–624
DOI 10.1007/s00396-011-2383-2

ORIGINAL CONTRIBUTION

Effect of cross-linker density of P(NIPAM-co-AAc) microgels at solid surfaces on the swelling/shrinking behaviour and the Young's modulus

Anna Burmistrova · Marcel Richter · Cagri Uzum · Regine v. Klitzing

Received: 26 November 2010 / Revised: 5 January 2011 / Accepted: 17 January 2011 / Published online: 12 February 2011

Abstract The effect of the amount of cross-linker in poly(*N*-isopropylacrylamide-co-acrylic acid) microgel particles on the swelling behaviour and their elasticity is studied. The distribution of the stiffness through the particle is also investigated. Therefore, the swelling ratio obtained from dynamic light scattering measurements in aqueous solutions is compared with the one after adsorption at polycation-coated silicon wafers. The studies of the swelling behaviour at the surface are carried out with scanning force microscopy (SFM) against liquid. The Young's modulus is determined by indentation experiments with an SFM. With increasing amount of cross-linker, the ability to shrink as well as the shift in the lower critical solution temperature and in particle size (hysteresis) during the heating and cooling processes decreases. In addition, the particles at the surface preserve their height/width ratio at high amount of cross-linker, while at low amounts the shrinking and swelling mainly takes place with respect to changes in height. The particles show their highest Young's modulus in the centre of the particles and become stiffer with increasing the amount of cross-linker and the temperature.

A. Burmistrova · M. Richter · C. Uzum · R. v. Klitzing (✉)
Institut fuer Chemie Stranski-Laboratorium,
Technische Universitaet Berlin, Strasse des 17. Juni 124,
10623, Berlin, Germany
e-mail: klitzing@mailbox.tu-berlin.de

A. Burmistrova
e-mail: burmistrova@mailbox.tu-berlin.de

M. Richter
e-mail: marcel.richter@tu-berlin.de

C. Uzum
e-mail: uzum@mail.tu-berlin.de

Keywords P(NIPAM-co-AAc) · Scanning force microscopy · Microgels

Introduction

Poly(*N*-isopropylacrylamide) (PNIPAM)-based microgels are the most investigated microgels in the last decades [1–5]. PNIPAM microgels typically have a lower critical solution temperature (LCST) at 32°C. This "smart" material finds applications in different areas such as drug delivery, emulsion stabilisation, microcontainer and switchable microlens preparation [6–10]. There are many publications investigating the induced responsive behaviour of microgels in volume phase [1, 4, 11–15]: the effect of ionic strength, pH, salt type, solvent quality and co-monomers on the swelling properties of PNIPAM-based microgels.

It was shown that the amount of cross-linker content strongly affects the microgel properties [16, 17]: The swelling ratio of microgels with higher cross-linker content is smaller than that of lower cross-linked microgels. The cross-linker amount also changes the internal structure of microgels. Microgels with higher cross-linker content demonstrate a core–shell-like structure: a core with high cross-linker density and a shell with lower cross-linker density. Due to their unique thermoresponsive properties, PNIPAM-based microgels have high potential to be used as functional surface coverage agents. There are several groups studying the adsorption properties of microgels and their ability to build close packed films [18–23].

The structural and mechanical properties of hydrogel films [24–28], single hydrogel particles [23, 29–32] or nanoribbons [33] were studied by either nanoin-

dentation or other techniques. The general trend observed is that together with the dramatic decrease in the particle size/film thickness, the stiffness increases as the temperature is increased. Matzelle and co-workers [24] observed a nearly 100-fold increase in the Young's modulus of swollen (10°C) and collapsed (35°C) PNIPAM hydrogel films. The effect of the cross-linking on the stiffness of PNIPAM films is also shown to be strong, especially in the collapsed state [25]. The effect of the cross-linking density, degree of ionization and the temperature on the elastic modulus of photo-cross-linked PNIPAM hydrogel layers was studied by Harmot and co-workers [26]. The authors observed a decreasing transition temperature as well as a broader transition range for higher cross-linking densities. Recently, Junk et al. have also reported a decrease in the swollen-collapsed transition temperature with increasing photo-cross-linking density [28]. They observed an exponential dependence of the elastic modulus on the polymer volume fraction for photo-cross-linked PNIPAM hydrogels. Atomic force microscope (AFM) indentation measurements for individual PNIPAM microparticles were found to show a similar behaviour as the hydrogel thin films, having 10–15-fold increase in the stiffness (Young's modulus) through the volume phase transition temperature [23, 29, 31], regardless of the cross-linker type and density. A stronger stiffness dependence (50-fold) on the temperature was calculated for ~25-nm-thick thermoresponsive nanoribbons [33]. It should be noted that the measured/calculated elastic moduli discussed above differ significantly from each other (form tens of pascals to hundreds of megapascals). But keeping in mind that the nature of the studied hydrogels are different in terms main components, cross-linker type and density and synthesis patterns, they show similar stiffness behaviours below and above the critical temperature. Another point to be noted is that the stiffness of the films shows a more or less homogeneous distribution both on x–y-plane and through the normal axis.

The current paper deals with the question how stiffness is distributed over a hydrogel microparticle and how the cross-linker density and the temperature affects it. For that purpose, thermoinduced swelling/shrinking behaviour of individually adsorbed poly(*N*-isopropylacrylamide-co-acrylic acid) (P(NIPAM-co-AAc)) microgels with different BIS content at different temperatures were investigated using the scanning and indentation properties of an atomic force microscope.

Experimental part

Microgel synthesis

Surfactant free emulsion polymerisation was used for the particle synthesis. *N*-Isopropyl acrylamide (NIPAM), *N*,*N*'-methylenebisacrylamide (BIS), potassium persulfate (PPS) and acrylic acid (AAc) were obtained from Sigma-Aldrich. All chemicals were used without further purification. The purity of NIPAM was at least 97%. Microgels with three different cross-linker contents were synthesised: MG1—2.26 g NIPAM, 0.072 g AAc and 0.06 g BIS (corresponding to 2% BIS with respect to the molar concentration of NIPAM monomers); MG2—2.27 g NIPAM, 0.072 g AAc and 0.15 g BIS (corresponding to 5% BIS) and MG3—2.27 g NIPAM, 0.072 g AAc and 0.31 g BIS (corresponding to 10% BIS) were dissolved in 200 ml Milli-Q water and placed under nitrogen atmosphere; 1.5 mg PPS was dissolved in 2 ml H_2O and added to the mixtures pre-heated to 70°C. After 4 h, the reaction was switched off via cooling down to room temperature. The cooled down solution was then stirred overnight under nitrogen atmosphere. Microgels were cleaned by 14-day dialysis in Milli-Q water. Water was exchanged daily. After cleaning, the microgels were freeze-dried. Microgels were deposited on the Si wafer covered with a gold layer of about 108 nm thickness (Georg Albert PVG-Beschichtungen) by spin coating with the microgel dispersions with a concentration of 0.05 wt.%. The rotation speed was 2,000 rpm and the deposition duration was fixed to 300 s. The coating was achieved under ambient conditions.

Methods

Dynamic light scattering

The swelling/deswelling behaviour of the microgels in volume phase was investigated by dynamic light scattering (DLS). The temperature range was between 15°C and 50°C. Intensity time auto-correlation functions were recorded at a constant scattering angle of 75° using an ALV goniometer setup. Using only one angle is justified by the high monodispersity of gel particles. A Nd:YAG laser with a wavelength of 532 nm, an output power 150 mW and an ALV-5000 correlator were used. The correlation functions were analysed by inverse Laplace transformation (CONTIN).

Scanning force microscopy

Scanning force microscopy (SFM) was used to characterise the swelling/shrinking behaviour of adsorbed microgels. All measurements were carried out with a JPK NanoWizard II in intermittent contact mode in an ECCell™ setup from JPK Instruments AG. Uncoated silicon cantilevers CSC37 from Micromash with a tip radius of ~10–50 nm were chosen as scanning probes. To get individual microgel particles deposited on the solid substrate, samples were prepared by spin coating from dispersions with a concentration of 0.05 wt.% as has been described above. Three types of measurements were done: (1) two long cycles. The temperature was changed between 15°C and 55°C in 5°C steps; (2) two short cycles. The temperature was changed between 20°C and 50°C in 15°C steps; and (3) two reswelling cycles. The samples were dried at room temperature overnight. After 12 h, the samples were deposited in water again and left for 1 h in liquid. The temperature was varied between 20°C and 50°C in 15°C steps during the measurements.

Elasticity measurements of microgels deposited at solid surfaces

The elasticity of the hydrogel particles was calculated using the force mapping tool with a measurement velocity of 0.3–1 Hz. Only the approach curves were used as there might be strong adhesion between the tip and the surface after the contact [23, 27]. V-shaped cantilevers (AR-iDrive-N01, Asylum Research, USA) with a reference spring constant of 0.09 N/m, carrying relatively blunt tips ($R \simeq$ 20–50 nm) were used for the scanning of surfaces and for force measurements. Selection of tips instead of colloidal probes prevents errors from insufficient indentation forces [24] and allows all scanning and force measurements to be done with the same tip without changing any parameter [28]. A modified form of the Hertz model suggested by Dimitriadis and coworkers [34] was used to calculate the Young's modulus individually at each indentation depth. According to that model, Young's modulus (E) is a function of force (F), indentation depth (δ), film thickness (h), indenter curvature (R) and the Poisson's ratio (v) and can be given with the general equation:

$$E = E(F, \delta, h, R, v) \quad (1)$$

It should be noted that the cantilever sensitivity should be calibrated on a clean, hard surface. This step is necessary to determine the hard-contact reference point and to record the correct cantilever deflection. In this study, the sensitivity calculations as well as the determination of the indentation depth were achieved by the JPK SFM software and home written Igor Pro (WaveMetrics, Inc., USA) procedures. Due to the electrostatic interactions between the hydrogel particles and the SFM tip, the force might be non-zero even before the contact, invalidating the assumption that $F = 0$ at $\delta = 0$. To determine the actual contact point, a region

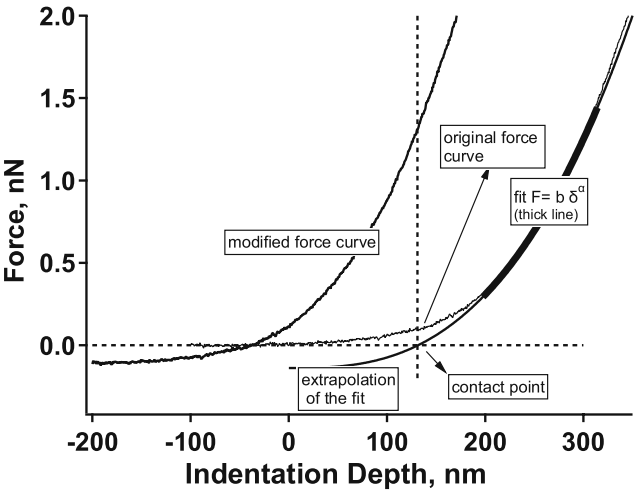

(a) Force vs Indentation Depth

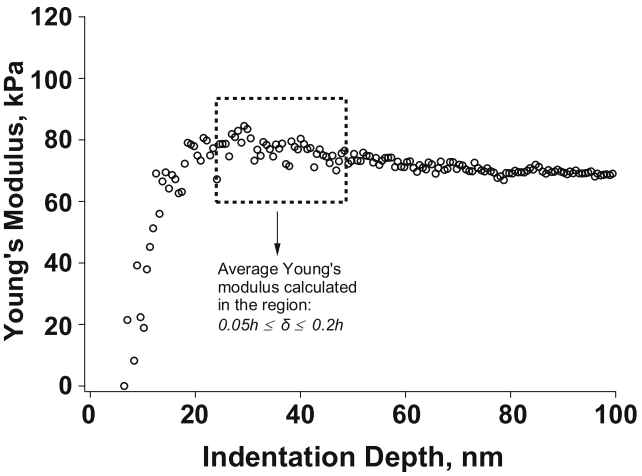

(b) Young's modulus vs Indentation Depth

Fig. 1 **a** Force as a function of indentation depth as measured by AFM, before and after the correction. **b** Young's modulus values calculated for each measurement point. The average Young's modulus is calculated from the region shown by the *box above*, h being the total film thickness

of the force–indentation curve where there is contact for sure is fit with the power law $F = y_0 + b\,\delta^{\alpha}$ with the constraint $3/2 \leq \alpha \leq 5/2$, where y_0 and b are non-essential parameters. The lower boundary of α (3/2) comes from the Hertz model itself. The upper boundary, 5/2, is an empirical value chosen to give reasonable contact points as higher α values would cause large deviations from the actual force curves. Actually, α should be changed depending on the strength of the electrostatic interactions and the softness of the measured surface. That fitting is assumed to give the force–indentation dependence including the further (weaker) electrostatic interactions after the contact. Extrapolating this fitting curve for $F = 0$ gives a reasonable contact point. Using the model of Attard [35], the exact contribution of the electrical double layer (EDL) on the interactions and deformation of the smooth surfaces can be determined. However, due to the porous nature of the hydrogels used in this study, Smoluchowsky equation cannot be used to calculate the exact EDL forces. An approximate calculation showed that the maximum EDL contribution is around 10% of the total force exerted on the cantilever at an indentation depth of 100 nm. It should be emphasized at this point that the electrostatic interactions cannot be ignored before and just after the contact. For the correction of the non-zero force at the new contact point determined by fitting, the force data were simply shifted down to satisfy $F = 0$ at $\delta = 0$. This step also removes the interference of any further electrostatic forces to the equation given below. The assumption is that there is no deformation before the contact, and the EDL interactions do not change dramatically after the contact.

For incompressible hydrogels ($v = 0.5$) that are bonded to the substrate, the extraction of the Young's modulus, E, can be achieved by calculating it for each indentation depth [34]:

$$E = \frac{9F}{16} \times \frac{1}{R^{1/2}\delta^{3/2}(1 + 0.884\chi + 0.781\chi^2 + 0.386\chi^3 + 0.0048\chi^4)} \quad (2)$$

where $\chi = \sqrt{R\delta}/h$. The force–indentation curves were taken from the force maps. The raw data were treated with self-made procedures on Igor Pro software from Wavemetrics, Inc.

The above relation necessitates a precise determination of h and R as they have dramatic effect especially for thin films [34]. The height of the hydrogel particles, h, was determined by scanning probe SFM and dynamic light scattering as has been discussed above. A spherical indentation geometry was assumed for the SFM tips, and the exact radii of curvature, R, were extracted from scanning electron microscope images.

Average Young's modulus in the indentation region $0.05\ \mathrm{h} \leq \delta \leq 0.2\ \mathrm{h}$ is used for the discussion of the results (see Fig. 1b). The Young's modulus is calculated for the sample temperatures of 20–50°C in 5°C steps. The fitting model is highly sensitive to the fitted δ range and to α, as well as to the particle height. This can result in relative errors up to 40% in the calculated Young's modulus. The ∓40% error bars are shown in the relevant graphs.

Results and discussions

Microgel characteristics in volume phase

Three types of microgel particles with different cross-linker contents were synthesised. The microgels in volume phase were characterised by DLS. They demonstrate the typical behaviour that the value of swelling ratio/particle volume (V) normalized with the volume at 15°C ($V^{15°C}$) decreases with increasing cross-linker content at high temperatures (Fig. 2). The LCST is determined from the point of inflection (Table 1).

Individually adsorbed microgels

To investigate the thermoresponsive shrinking and swelling behaviour of individually adsorbed microgels, the SFM technique in liquid was used. Figure 3 shows the SFM images of microgels with 2% BIS content

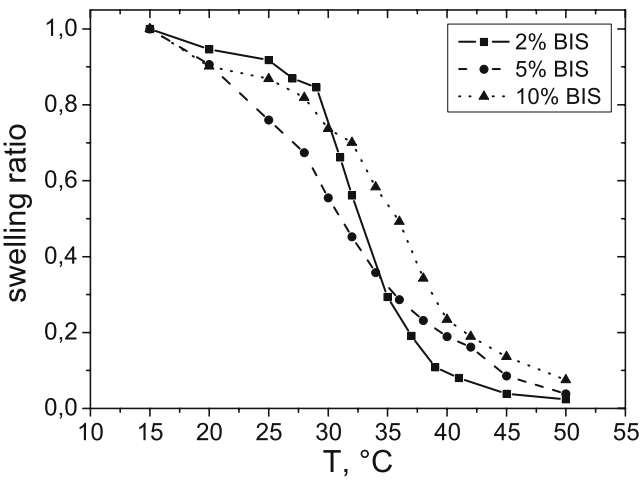

Fig. 2 Swelling ratio of microgels in bulk as function of temperature for microgels with 2% (*squares*), 5% (*circles*) and 10% (*triangles*) BIS contents

Table 1 Characteristics of microgels in bulk: the LCST and swelling ratio; deposited at the surface: LCST, swelling ratio and height/width ratio at 20°C and 50°C and volume of microgels in bulk normalized with respect to the volume of adsorbed microgels at 15°C and at 50°C

BIS content (%)	Volume phase		Adsorbed microgels				V_{DLS}/V_{SFM} at 15°C	V_{DLS}/V_{SFM} at 50°C
	$LCST_{DLS}$ (%)	Swelling ratio at 50°C	$LCST_{SFM}$ (%)	Swelling ratio at 50°C	Height/width ratio at 20°C	Height/width ratio at 50°C		
2	33	0.29	35	0.19	0.21	0.07	10	1.1
2	30	0.34	37	0.29	0.26	0.1	9.7	1.3
10	35	0.42	33	0.47	0.46	0.48	7.2	1.1

Characteristics for deposited particles were taken from the heating process of the second long cycle

during the first long cycle: 15°C, 35°C, 55°C, 35°C and 15°C. The obvious change in the microgel size can be seen. In order to get a better insight into the swelling ratio, the volume of deposited particles was calculated from cross sections [36] and is shown in Fig. 4. The process does not seem to be completely reversible. Microgels with 2% cross-linker show a strong shift (hysteresis) in the LCST and in particle size during the first long cycle. The LCST at the cooling process is shifted by 2.2–34.4°C with respect to the heating curve. After the cooling process in the first long cycle, the microgel height and the footprint become smaller than those before the heating process; at 15°C, particle volume changes from 1.2×10^8 to 7.6×10^7 nm^3. During the second long cycle, the LCST is again shifted by 2.1–32.6°C, and the hysteresis significantly decays after the second long cycle. With the increasing cross-linker content, the hysteresis decreases and the slope around the point of inflection increases, i.e. the transition becomes sharper. After the hysteresis vanishes, the LCST becomes similar to the one of microgel particles in aqueous dispersion. This is in good agreement with the former studies [20, 37] and is explained by the dominating effect of the chemically cross-linked gel material. In contrast to that, films of physically cross-linked PNIPAM gels show a strong effect of the film thickness on the LCST, resulting from confinement or substrate influences [38].

Cheng et al. [39] showed that PNIPAM homopolymers are able to build intra- and inter-polymer chain hydrogen bonds during the heating process. The H-bonds can be broken during a subsequent cooling process down to a temperature of about 4°C. In the present experiment, the microgels were cooled down to 15°C and the H-bonds were observed not to disappear completely. These remaining H-bonds can be considered as new additional cross-linkers. Due to these new cross-linkers, the particles cannot swell to their initial sizes and the hysteresis takes place. With increasing BIS content, the chain length between two cross-linkers decreases and the intrachain hydrogen bonds could not be formed during the heating process, and the hysteresis becomes smaller and vanishes, respectively.

In order to compare the effect of cross-linker on the swelling/shrinking behaviour, the swelling ratio of all three gel particles after adsorption at the Si/Au substrate is shown in Fig. 5. The adsorbed particles demonstrate qualitatively the similar behaviour to microgels in the volume phase: with increasing BIS content the swelling ratio of adsorbed microgels decreases.

To check whether the hysteresis totally disappears after the first few cycles, two short cycles between 20°C and 50°C with 15°C steps were driven. The volume normalized with respect to the particle volume at 20°C in the first short cycle is shown in Fig. 6. It was observed that all three types of microgels adsorbed on

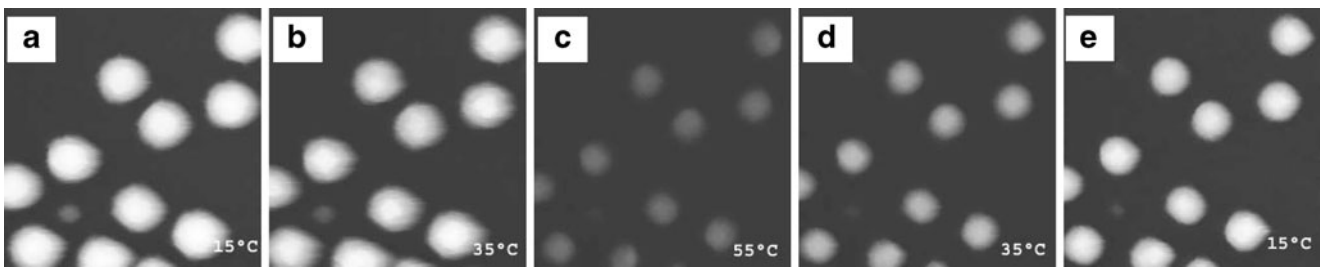

Fig. 3 SFM images against water of adsorbed microgels with 2% BIS in the first long cycle: at 15°C (**a**), 35°C (**b**), 55°C (**c**), 35°C (**d**) and 15°C (**e**). Measurements were carried out in intermittent mode

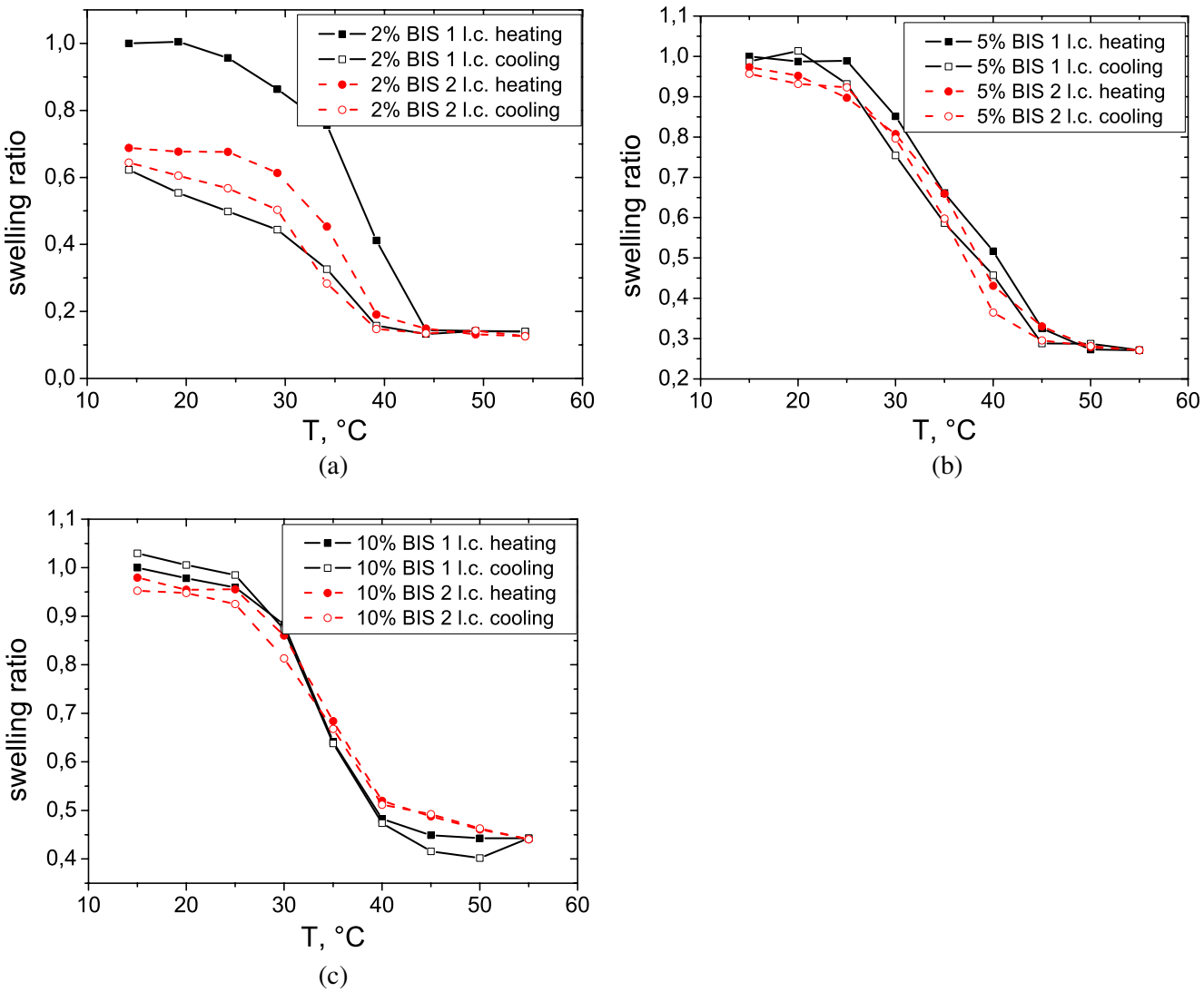

Fig. 4 Swelling ratio of adsorbed microgels with 2% (**a**), 5% (**b**) and 10% (**c**) BIS contents in the first and second long cycles as function of temperature measured by SFM

the surface had a reversible thermoinduced behaviour. The shift in the LCST and in the particle size decreases in cooling and heating processes in the second long cycle (see Fig. 4a and Table 1). The adsorbed microgels demonstrate the thermoresponsive behaviour in reswelling experiments as well. To show that, the samples were dried at room temperature overnight. For SFM measurements, the sample was left in liquid to reswell. After 1 h, the SFM measurements were performed. No microgel particle desorption could be observed during the reswelling process. It should be noted that the microgels deposited on the solid surface still exhibit the swelling/shrinking behaviour even after a complete sample drying.

The characteristics of microgel particles such as the LCST, swelling ratio of microgels in bulk; the LCST in the heating process of the second long cycle, the swelling ratio and the height-to-width ratio at 20°C and at 50°C of adsorbed microgels and the ratio of particle volume in bulk to the volume of deposited on the Si/Au microgels are given in Table 1.

The values of V_{DLS}/V_{SFM} in swollen state or at 15°C indicate that the internal density of the particles deposited at the surface is higher than that of the particles in bulk. This ratio decreases with increasing cross-linker content due to decreasing polymer chain length between two cross-linker and as consequence increasing particles stiffness. With increasing temperature up to 50°C, the ratio decreases. At this temperature, particles are in the collapsed state and the chain length between two BIS molecules is extremely short, leading to a decrease in this ratio.

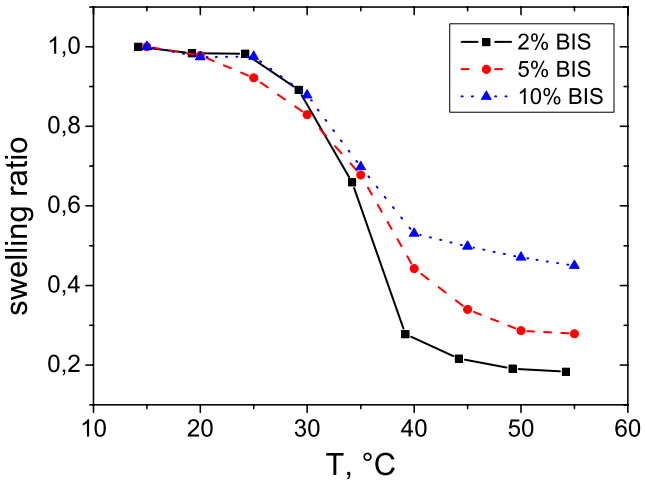

Fig. 5 Swelling ratio of adsorbed microgels with 2% BIS (*squares*), 5% BIS (*circles*) and 10% BIS (*triangles*) got by SFM for the heating process in the second long cycle as function of temperature

The height/width ratio of adsorbed particles increases with increasing BIS content showing that the particles become stiffer with increasing BIS concentration. The height/width ratio at 50°C is significantly smaller than that at 20°C for the particles with lower cross-linker content because the collapse of adsorbed microgels takes place mainly in vertical direction. In case of 10% BIS, this ratio is almost temperature independent indicating the preservation of particle shape in heating and cooling processes and is also indicated much smaller shrinking (0.47) compared to particles with lower BIS contents (0.19 for 2% BIS and 0.29 for 5% BIS). This result shows that microgels with 10% BIS possess a hard particle like behaviour. The schematic thermoinduced shrinking process is shown in Fig. 7. The lower cross-linked microgels collapse mainly in vertical direction and the particles shape changes: becomes flatter. The higher cross-linked microgels collapse in vertical as well as in horizontal directions and keep their shape. Due to the higher internal density of adsorbed microgels compared to microgels in bulk, the transition of deposited particles becomes sharper (Figs. 2 and 5). The LCST of the microgels at surface tends to be higher than in volume phase. The swelling ratio of gel particles in bulk and adsorbed at the surface increases with increasing BIS content indicating a decreasing swelling ability. To get quantitative information about the "hardness" of the particles deposited on the solid surface, SFM measurements were carried out as the temperature and the BIS content were varied.

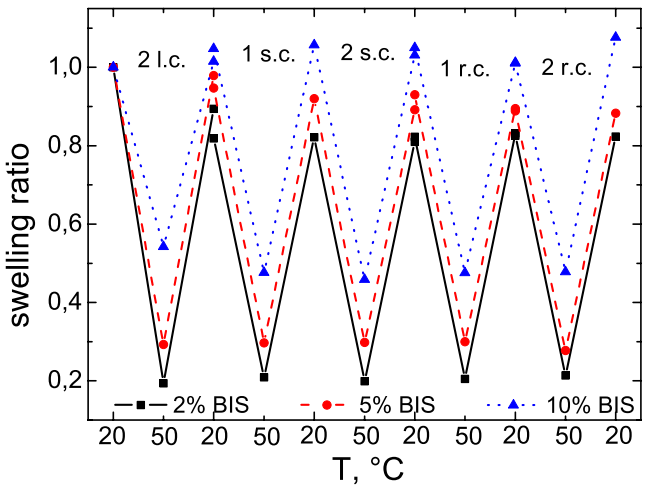

Fig. 6 The swelling ratio of adsorbed microgels with 2% BIS (*squares*), 5% BIS (*circles*) and 10% BIS (*triangles*) at 20°C and 50°C in different heating/cooling cycles: in the second long cycle (2 l.c.), in the first and in the second short cycle (1 and 2 s.c.) and in the first and in the second reswelling cycle after drying (1 and 2 r.c.)

Elasticity measurements

To determine the temperature dependence of the Young's modulus, the microgel particle in question was scanned, and the image was subdivided into squares by a grid for the force mapping (Fig. 8). The adhesion in the retraction process in the force measurements was never let to be too strong as it can otherwise irreversibly damage the microgels [23]. Grids 1–7 in Fig. 8 were analysed throughout three heating–cooling cycles. Different approach speeds (0.3–1 Hz) were used in the force measurements. A systematic study about the effect of measurement velocity (0.5–7 Hz) had already showed that the Young's modulus does not vary more than 10% in that velocity range [31] for a similar system. That is why any possible viscous behaviour of the hydrogels were neglected throughout this study.

For a better understanding of the material distribution in the hydrogel particles, the Young's Moduli were determined through the line in Fig. 8 (grids 1–7). Young's modulus values at 20°C and at 50°C, corresponding to the height cross section from scanning probe AFM, are given in Fig. 9a, b for 2% and c, d for 10% cross-linked particles at 20°C and 50°C, respectively. It can be clearly seen that for both hydrogels, the Young's modulus reaches a maximum in the middle of the particle. Towards the rim of the particle (for example, points 3 and 5 in Fig. 8), there is a 2–5-fold decrease in the stiffness. This behaviour can be attributed to the previously suggested morphology of the hydrogel particles, meaning that there is less material at the outer regions of the particle and stiffening cross-linkers are concentrated in the middle (or core; see Fig. 12).

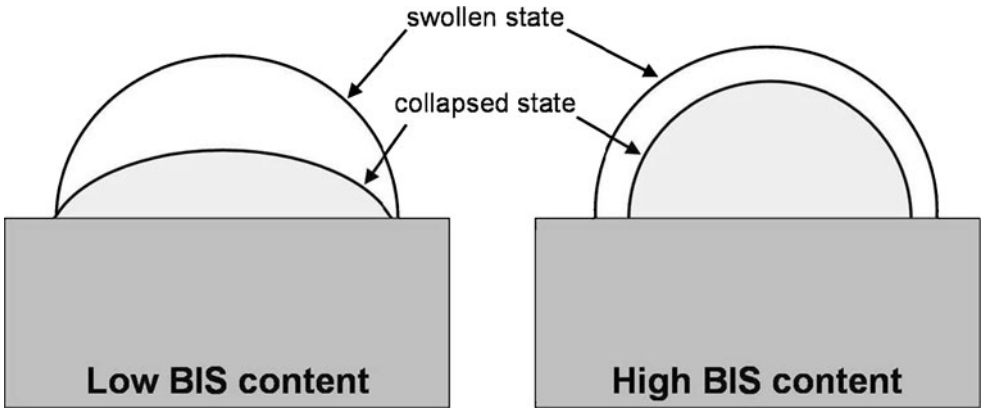

Fig. 7 Scheme of the shrinking process for particles with low and high cross-linker contents

As less dense material would be softer, the Young's modulus of the outer regions is expected to be much smaller than that of the centre. The elastic modulus difference between the outer periphery and the centre is more pronounced at higher temperatures and for the higher cross-linked particles. Due to this inhomogeneous character of the microgels, a major problem in the interpretation of the data might arise. As Hertz-based models assume a homogeneous structure, the calculated Young's modulus values should be checked against any abrupt changes for different indentation depths. It should also be stressed that different film heights at different spots on the particle have to be considered while calculating the Young's modulus with Eq. 2.

The Young's modulus in the middle of the particle (see grid 4 in Fig. 8) was obtained by averaging the calculated Young's Moduli in an indentation depth of

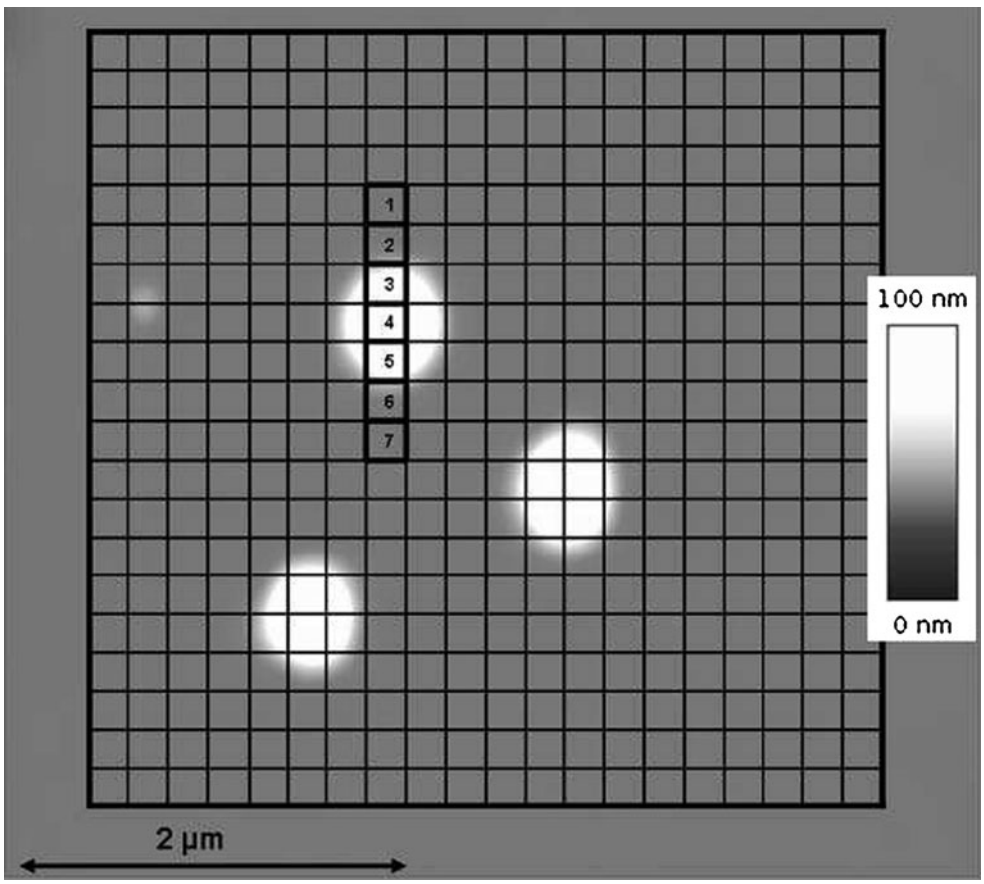

Fig. 8 The microgels as imaged by SFM. The grids correspond to the force measurement spots on the force mapping

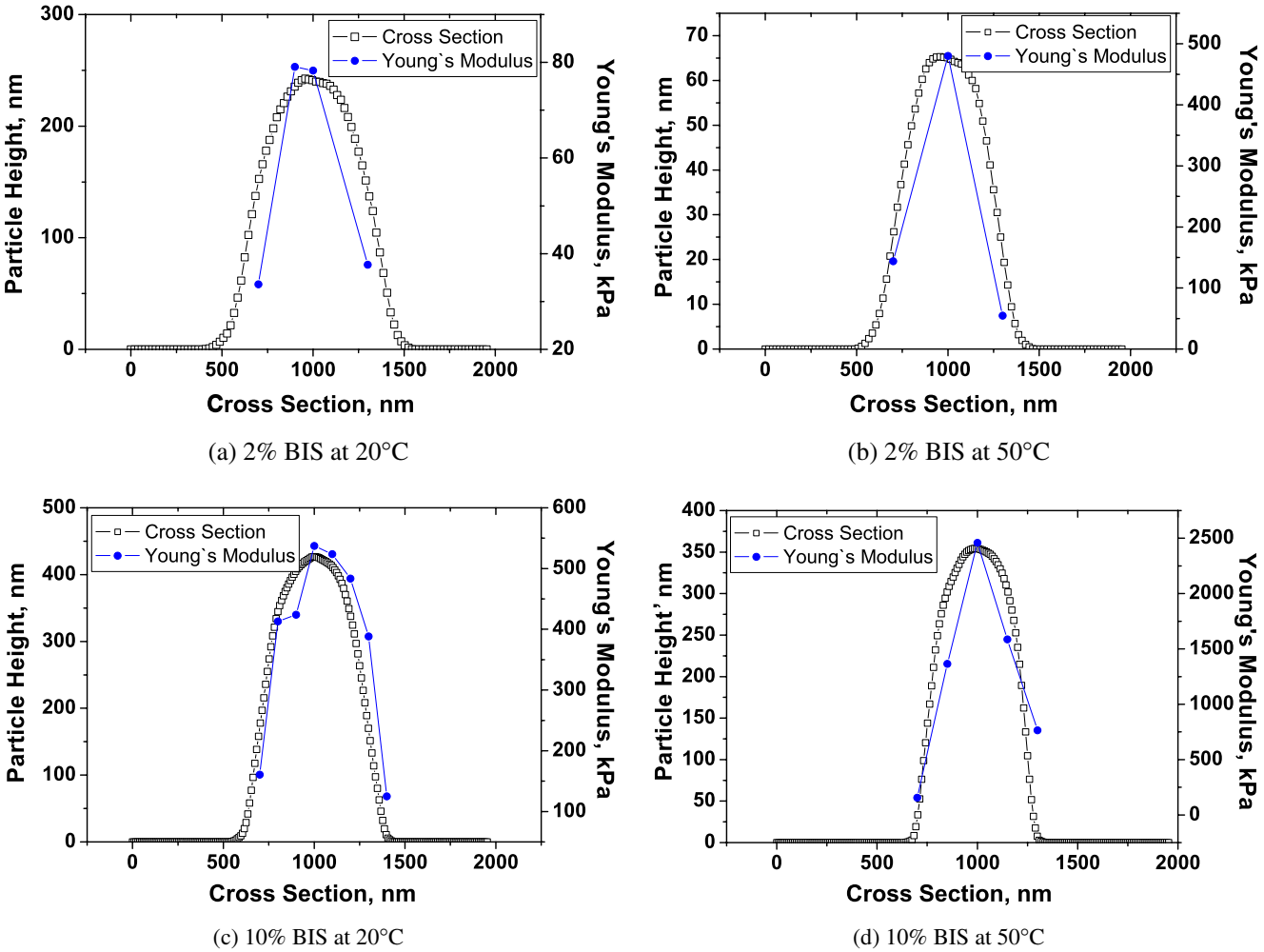

Fig. 9 Thickness and Young's modulus dependence on the cross-section position for particles with 2% and with 10% BIS at 20°C and at 50°C

5–20% of the total particle height as shown in Fig. 1b. The average values for MG1 and MG3 are given in Fig. 10. It was observed that the Young's modulus (as a measure of stiffness) of the particles does not change in the temperature range of 20–35°C. A constant or slowly increasing modulus trend below the critical solubilization temperature has been observed previously for hydrogel films and particles, despite different temperature ranges [24, 26, 27, 31, 33, 40]. There is a continuous increase in the stiffness from 35°C to 50°C. As no plateau could be reached in that temperature range, additional measurements in a wider temperature range of 20–70°C were run. Figure 11 shows the relative Young's modulus values for both 2% and 10% cross-linked microgels. A 5- to 6-fold increase from the lowest to the highest temperature can be seen. Again a 6-fold increase in the elastic modulus occurs as the cross-linker density is increased five times, from 2% to 10%. This trend is expected as the 10% BIS particle is more compact and stiffer due to the highly cross-linked polymer network as has been previously observed for similar systems [25, 26, 28]. But it should be noted that despite its stiffer structure, 10% BIS follows the similar temperature dependence trend as the lower cross-linked hydrogel (2% BIS).

It can be seen in Fig. 11 that the critical temperature is between 35°C and 50°C for both samples. For the 2% cross-linked particles, a decrease in the modulus can be observed around 40°C (Figs. 10a and 11). A decrease in the elastic modulus close to the phase transition temperature was also reported by Hashmi and Dufresne [31]. That gives a clue for the critical temperature of the 2% cross-linked sample (~40°C). This temperature is at least more than 5°C higher than the LCST determined by SFM and DLS. So the critical changes in stiffness and in size occur with a temperature

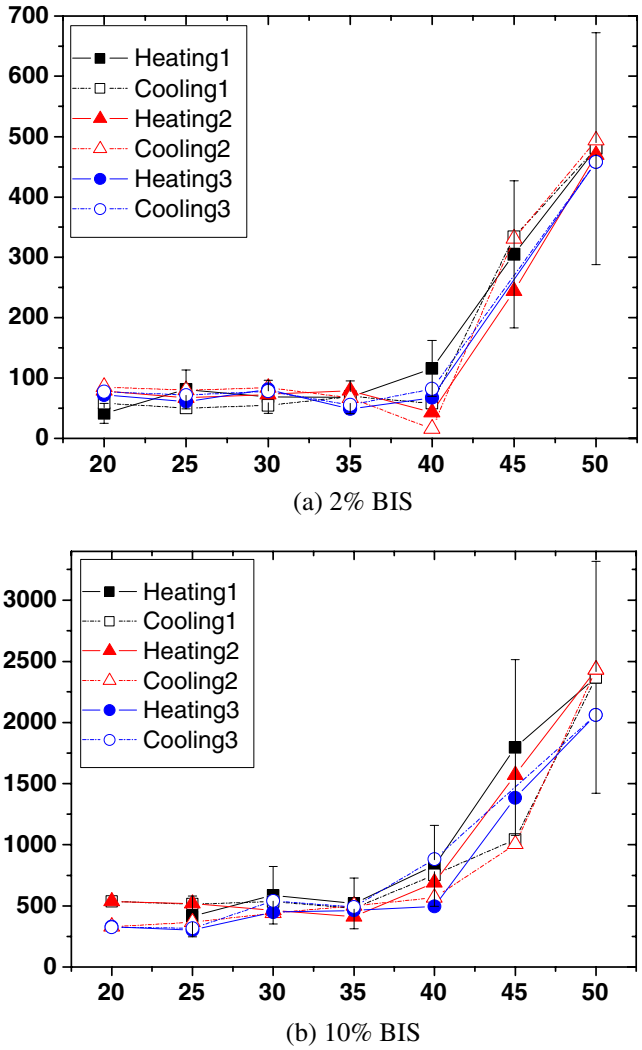

Fig. 10 Temperature dependence of the Young's modulus for adsorbed microgel particles with 2% and 10% cross-linker content. Measurements were carried out in the center of the particles (grid 4 in the Fig. 8). *Error bars* indicate 40% relative errors

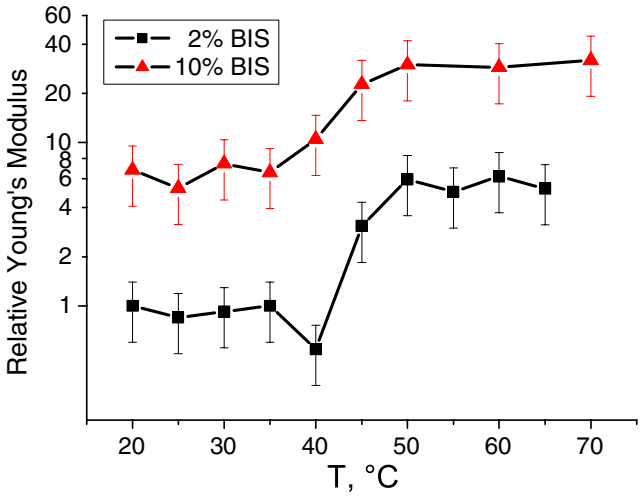

Fig. 11 The calculated Young's modulus values in logarithmic scale as normalized to the value for the 2% cross-linked hydrogel at 20°C. The *error bars* indicate 40% relative errors

shift. The possible reason for this sort of behaviour is also related to the unexpected lack of hysteresis in the elastic modulus through the heating–cooling cycles, as will be discussed below.

Varga et al. [17] have shown that as the first step, a cross-link rich core was formed during the synthesis. As the BIS concentration in the reaction mixture decreases, the branched PNIPAM polymer chains are built and the shell with a low cross-link density is formed. In the temperature-induced transition process, the microgel structural changes occur in several steps [11]: In the first step, the initial core collapse takes place (the thickness decreases but the lower cross-linked region, of which elasticity is measured, keeps its softness. Critical temperature for the particle size is reached in this step). In the second step, the shell collapses (letting the AFM tip to reach the stiffer core. Partial increase or decrease in the elasticity can be observed). In the third step, the core collapses again (the size decreases only slightly but the stiffness of the higher cross-linked region increases dramatically. The critical temperature for the elasticity is reached).

One can expect from the SFM measurements (Fig. 4) that during the heating–cooling cycles, the Young's moduli of lower BIS content microgel particles would also have a hysteresis. In contrast to that, Fig. 10 demonstrates no hysteresis. This can be attributed to the significant difference between the core and the shell in terms of softness. In the force measurements at high temperatures, the tip penetrates the relatively softer shell without giving any significant deflection signal compared to the harder core, invalidating any deformation theory. The only elastic behaviour that can be measured at this point is the deformation of the higher cross-linked core (Fig. 12). Due to the absence of a hysteresis, it can be suggested that no significant change takes place in the particle core throughout the cycles but only in the lower cross-linked outer rim. So the core has the same structure at a certain temperature independent of how many times it has been exposed to a heating–cooling cycle. This phenomenon indicates that the previously discussed H-bonding takes place mostly in the lower cross-linked particle periphery.

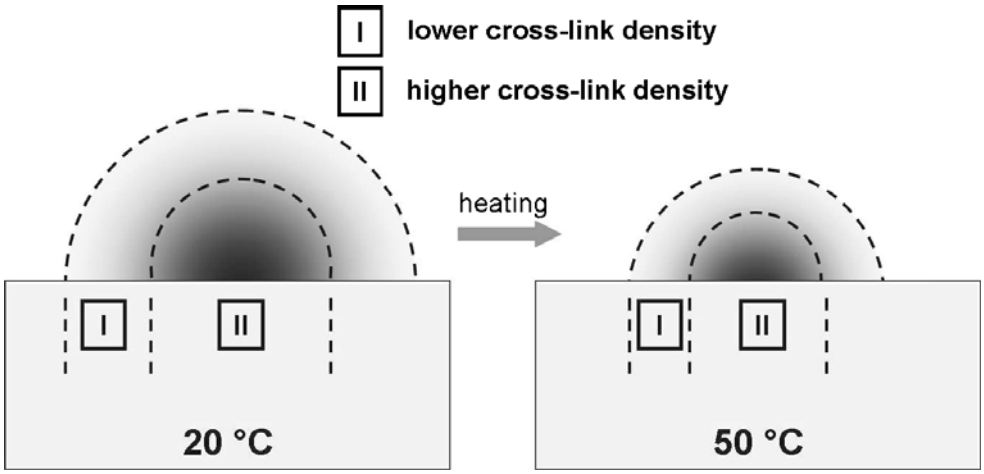

Fig. 12 Scheme of the shrinking process of microgel particles deposited at a solid surface

Conclusions

(1) The thermoinduced swelling behaviour was compared between microgels in bulk and after adsorption on the surface. For both, the swelling ratio decreases with increasing of cross-linker content. (2) Reversible swelling/shrinking behaviour during several cycles was observed and hysteresis decreases with increasing BIS content. (3) Microgels deposited at solid interface have higher internal density than the microgels in bulk. After the adsorption, low cross-linked particles become flat in heating processes. The shape of high cross-linked microgels is invariant in swelling/shrinking processes. (4) The highest Young's modulus was observed in the centre of the microgel particle. (5) The Young's modulus increases with increasing cross-linker content and heating through the LCST. (6) The fact that no hysteresis in the Young modulus could be observed indicates that the formation of H-bonds during the first cycles occurs in the particle's low cross-linked shell.

Acknowledgements The authors thank TU Berlin and German Research Council (DFG) for the financial support via the priority program 1259 "Intelligente Hydrogele" (KL1165-7/1 and 2) and CoE UniCat.

References

1. Kratz K, Eimer W (1998) Ber Bunsenges Phys Chem 102(6):848
2. Sierra-Martin B, Romero-Cano MS, Fernandez-Nieves A, Fernandez-Barbero A (2006) Langmuir 22(8):3586
3. Hoare T, Pelton R (2004) Macromolecules 37:2544
4. Karg M, Pastoriza-Santos I, Rodriguez-Gonzalez B, von Klitzing R, Wellert S, Hellweg T (2008) Langmuir 24(12):6300. doi:10.1021/la702996p. URL: http://pubs.acs.org/doi/abs/10.1021/la702996p. PMID: 18489184
5. Meng Z, Cho JK, Breedveid V, Lyon LA (2009) J Phys Chem B 113:4590
6. Hoare T, Perlton R (2008) Langmuir 24:1005
7. Yin Z, Zhang J, Jiang LP, Zhu JJ (2009) J Phys Chem C 113:16104
8. Ngai T, Behrens SH, Auweter H (2005) Chem Commun 3:331–333
9. Kim J, Serpe MJ, Lyon LA (2004) J Am Chem Soc 126:9512
10. Kim J, Nayak S, Lyon LA (2005) J Am Chem Soc 127:9588
11. Daly E, Saunders BR (2000) Phys Chem Chem Phys 2:3187
12. Daly E, Saunders BR (2000) Langmuir 16:5546
13. Hellweg T (2003) Properties of NIPAM-based intelligent microgel particles. Kluwer, Boston
14. Larsson A, Kuckling D, Schoenhoff M (2001) Colloid Surf A Physicochem Eng Asp 190:185
15. Rasmusson M, Routh A, Vincent B (2004) Langmuir 20:3536
16. Sierra-Martin B, Choi Y, Romero-Cano MS, Cosgrove T, Vincent B, Fernandez-Barbero A (2005) Macromolecules 38:10782
17. Varga I, Gilanyi T, Meszaros R, Filipcsei G, Zrinyi M (2001) J Phys Chem B 105(38):9071. doi:10.1021/jp004600w. URL: http://pubs.acs.org/doi/abs/10.1021/jp004600w
18. Nerapusri V, Keddie JL, Vincent B, Bushnak IA (2006) Langmuir 22:5036
19. Schmidt S, Hellweg T, von Klitzing R Langmuir (2008) 24(21):12595. doi:10.1021/la801770n. URL: http://pubs.acs.org/doi/abs/10.1021/la801770n. PMID: 18847289
20. Schmidt S, Motschmann H, Hellweg T, von Klitzing R (2008) Polymer 49(3):749. doi:10.1016/j.polymer.2007.12.025
21. Hellweg T, Dewhurst CD, Brueckner E, Kratz K, Eimer W (2000) Colloid Polym Sci 278:972
22. Sorrell CD, Lyon LA (2007) J Phys Chem B 111:4060
23. Wiedemair J, Serpe MJ, Kim J, Masson JF, Lyon LA, Mizaikoff B, Kranz C (2007) Langmuir 23:130
24. Matzelle T, Ivanov D, Landwehr D, Heinrich L, Herkt-Bruns C, Reichelt R, Kruse N (2002) J Phys Chem B 106(11):2861. doi:10.1021/jp0128426

25. Matzelle T, Geuskens G, Kruse N (2003) Macromolecules 36(8):2926. doi:10.1021/ma021719p
26. Harmon M, Kucking D, Frank C (2003) Langmuir 19(26):10660. doi:10.1021/la030232m
27. Cheng X, Canavan H, Stein M, Hull J, Kweskin S, Wagner M, Somorjai G, Castner D, Ratner B (2005) Langmuir 21(17):7833
28. Junk MJN, Berger R, Jonas U (2010) Langmuir 26(10):7262. doi:10.1021/la903396v
29. Tagit O, Tomczak N, Vancso GJ (2008) Small 4(1):119. doi:10.1002/smll.200700260
30. Banquy X, Zhu XX, Giasson S (2008) J Phys Chem B 112(39):12208. doi:10.1021/jp803605d
31. Hashmi SM, Dufresne ER (2009) Soft Matter 5(19):3682. doi:10.1039/b906051k
32. Banquy X, Suarez F, Argaw A, Rabanel JM, Grutter P, Bouchard JF, Hildgen P, Giasson S (2009) Soft Matter 5(20):3984. doi:10.1039/b821583a
33. Radji S, Alem H, Demoustier-Champagne S, Jonas AM, Cuenot S (2010) J Phys Chem B 114(15):4939. doi:10.1021/jp909819h
34. Dimitriadis E, Horkay F, Maresca J, Kachar B, Chadwick R (2002) Biophys J 82(5):2798
35. Attard P (2007) J Phys Condens Matter 19(47):473201. doi:10.1088/0953-8984/19/47/473201
36. Burmistrova A, Steitz R, von Klitzing R (2010) ChemPhysChem 11(17):3571. doi:10.1002/cphc.201000378
37. Burmistrova A, von Klitzing R (2010) J Mater Chem 20(17):3502
38. Wang W, Troll K, Kaune G, Metwalli E, Ruderer M, Skrabania K, Laschewsky A, Roth SV, Papadakis CM, Mueller-Buschbaum P (2008) Macromolecules 41(9):3209. doi:10.1021/ma7027775
39. Cheng H, Shen L, Wu C (2006) Macromolecules 39:2325
40. Liu K, Ovaert TC, Mason JJ (2008) J Mater Sci Mater Med 19(4):1815. doi:10.1007/s10856-007-3325-x